AMERICAN SCIENTIFIC PUBLISHERS

Journal of Nanofluids
Vol. 6, pp. 883–891, 2017
(www.aspbs.com/jon)

ARTICLE

MHD Boundary Layer Heat and Mass Transfer Flow Over a Vertical Cone Embedded in Porous Media Filled with Al_2O_3-Water and Cu-Water Nanofluid

B. Prabhavathi[1], P. Sudarsana Reddy[1,*], R. Bhuvana Vijaya[2], and Ali. J. Chamkha[3]

[1]*Department of Mathematics, Rajeev Gandhi Memorial College of Engineering and Technology, Nandyal 518501, India*
[2]*Department of Mathematics, Jawaharlal Nehru Technological University, Anantapur 515001, India*
[3]*Department of Mathematics, Prince Mohammad Bin Fahd University, Al-Khobar, 31952, Saudi Arabia*

We have presented a numerical solution to the MHD boundary layer heat and mass transfer flow of Al_2O_3-water and Cu-water based nanofluids over a vertical cone saturated by porous media with heat generation/absorption, thermal radiation and chemical reaction in the present analysis. Though we have different varieties of nanofluids, we have considered Al_2O_3-water and Cu-water based nanofluids (with volume fraction 1% and 4%) in this problem. The governing partial differential equations describing the steady-state conservation of mass, momentum, energy as well as conservation of nanoparticles for nanofluids are transformed into the set of ordinary differential equations by using suitable similarity transformations and are solved numerically subject to the boundary conditions using an efficient, extensively validated, variational Finite element method. The influence of important non-dimensional parameters on velocity, temperature and nanoparticle concentration fields as well as the skin-friction coefficient, Nusselt number and Sherwood number are examined in detail and the results are shown in graphically and in tabular form to illustrate the physical importance of the problem.

KEYWORDS: Al_2O_3-Water and Cu-Water Nanofluid, MHD, Thermal Radiation, Heat Generation/Absorption, Chemical Reaction.

1. INTRODUCTION

Nanofluids are novel category of heat transferred fluids, containing nano-meter sized (1–100 nm) particles called nanoparticles that are being used to enhance the thermal conductivity of the base fluids like water, ethylene glycol, toluene, and engine oil.[1] Nanofluids have been employed in different fields of thermal engineering such as heat exchangers, nuclear reactors and cooling of electronic devices.[2] Several researches have worked on higher natural convection heat transfer capabilities of nanofluid, among all Choi[3] was the first among all who introduced a new type of fluid called nanofluid while doing research on new coolants and cooling technologies. Eastman et al.[4] have noticed in an experiment that the thermal conductivity of the base fluid (water) has increased up to 60% when CuO nanoparticles of volume fraction 5% are added to the base fluid. Eastman et al.[5] have also showed that the thermal conductivity has increased 40% when copper nanoparticles of volume fraction less than 1% are added to the ethylene glycol or oil. Choi et al.[6] have reported that there is 150% enhancement in thermal conductivity when carbon nanotubes are added to the ethylene glycol or oil. In addition, Xie et al.[7] have observed that Al_2O_3-ethylene glycol based nanofluid thermal conductivity is increased in the range 25–30% when Alumina nanoparticles are added. In his bench mark study, Buongiorno[8] has reported seven possible mechanisms associating nanofluid natural convection through moment of nanoparticles in the base fluid using scale analysis. Putra et al.[9] have found in their experimental investigation that in the both Al_2O_3-water and CuO-water based nanofluids there is remarkable heat transfer decrement when the volume fraction of nanoparticle is 1%–4%. Wen and Ding[10] also noticed natural convection heat transfer deterioration in TiO_2-water based nanofluids (with volume fraction 0.19% and 0.57%) in their study. Li and Peterson[11] have described natural convection heat transfer deceleration in the Al_2O_3-water based nanofluid (with volume fraction 0.5% and 6%) and is because of nanoparticle Brownian motion smoothing the temperature gradient causes delay in natural convection. Rui et al.[12] noticed deterioration in natural convection heat transfer in the Al_2O_3-water based nanofluid and is due to mass diffusion of nanoparticles in their experimental study

*Author to whom correspondence should be addressed.
Email: suda1983@gmail.com
Received: 2 February 2017
Accepted: 13 March 2017

under the Rayleigh-Benard configuration. Nnanna et al.[13] have found in their experiment that the natural convection heat transfer depreciates when nanoparticle volume fraction is more than 2% in the Al_2O_3-water based nanofluid and is owing to increase of kinematic viscosity. Ho et al.[14] also conveyed up to 18% natural convective heat transfer improvement Al_2O_3-water nanofluid (with volume fraction 0.1%), but deterioration was found when the volume fraction was more than 0.2. Ghalambaz et al.[15] have noticed depreciation in the rates of heat transfer of nanofluid with the increasing values of Brownian motion and buoyancy ratio parameters.

Recently, Lervik et al.[16] have presented numerical studies to analyze the possible heat transfer mechanisms between nanoparticle and fluid. Abu-Nada et al.[17] have analyzed natural convection heat transfer enhancement in a horizontal concentric annuli filled with nanofluid. Eliodoro et al.[18] have analyzed water passage through nanoconfined geometries using scale analysis. Khanafer et al.[19] found remarkable heat transfer enhancement in CuO-water based nanofluids when nanoparticle volume fraction is up to 20%. Oztop and Abu-Nada[20] have deliberated heat and mass transfer characteristics of three different nanofluids, namely, Al_2O_3-water, TiO_2-water and CuO-water, over rectangular enclosures and they noticed significant natural heat transfer enhancement when volume fraction of nanoparticles is up to 20%. Aminossadati and Ghasemi[21] reported that the cooling performance of pure water in a bottom-heated two-dimensional enclosure could improve when adding copper (Cu), silver (Ag), Al_2O_3 and TiO_2 nanoparticles (φ was up to 20%). Ghasemi and Aminossadati[22] have perceived notable enhancement in the rates of heat transfer over a triangular cavity filled with CuO-water nanofluid when the volume fraction (φ) of nanoparticle is 0.01 to 0.04. Fakhreddine Segni et al.[23] found nanofluid natural convection heat transfer enhancement in a two-dimensional cavity filled with Al_2O_3, TiO_2 and Cu nanoparticles when the volume fraction of nanoparticles is less than 0.05. Ternik et al.[24] studied the heat transfer enhancement of water-based gold (Au), Al_2O_3, Cu and TiO_2 nanofluids when (φ) was up to 10% in a two dimensional cavity. Recently, Chamkha et al.[25–27] deliberated MHD boundary layer flow, heat and mass transfer characteristics of different nanofluids over various geometries, like, wedge, cone, vertical cone with the influence of thermal radiation first order chemical reaction, etc. Noghrehabadi et al.[28–30] have analyzed the natural convection of nanofluids under different geometries stretching sheet, vertical plate respectively. Behseresht et al.[31] have presented natural convection heat and mass transfer of nanofluid over a vertical cone by taking the practical range of nanofluids thermo-physical properties. Recently, Rasad et al.[32] have analyzed natural convection non-Darcy nanofluid over a vertical cone through porous medium. Ghalambaz et al.[33] reported the influence of nanoparticles diameter and concentration over a vertical cone though porous media filled with Al_2O_3-water nanofluid with variable thermal conductivity. In their study the rates of heat transfer enhances when the volume fraction of nanoparticle is 0.02–0.04. Reddy et al.[34] have noted natural convection heat transfer deterioration in the both Al_2O_3-water and Ag-water based nanofluids over a vertical cone in their numerical study. Noreen Sher Akbar et al.[35] have discussed the peristaltic flow of carbon nanotubes over permeable channel under the impact of magnetic field and heat flux. Sheikholeslami et al.[36] have presented convective heat transfer analysis of Cuo-water nanofluid by considering Lorentz forces. Sheikholeslami et al.[37] have deliberated two phase model flow and heat transfer of nanofluid with thermal radiation.

To the best of authors' knowledge, no studies have been found in literature to study the influence of nanoparticle volume fraction (ϕ) and Magnetic field on flow, heat and mass transfer characteristics over a vertical cone through porous medium filled with Al_2O_3-water and Cu-water based nanofluids. Hence, this problem is addressed in this article.

2. MATHEMATICAL FORMULATION

Figure 1 demonstrates a two-dimensional, study, electrically conducting heat and mass transfer flow of nanofluid about a vertical cone placed in Darcy porous medium. The coordinate system is chosen as the x-axis is aligned with the flow direction on the cone. It is assumed that T_w, and ϕ_w are the temperature and nanoparticle volume fraction at the surface of the cone ($y = 0$) and T_∞ and ϕ_∞ are the temperature and nanoparticle volume fraction of the ambient fluid, respectively. An external magnetic field of strength B_0 is applied in the direction of y-axis. The thermo-physical properties of different nanoparticle are listed in Table I. By considering the works of Kuznetsov and Neild[38] and by employing the Oberbeck-Boussinesq

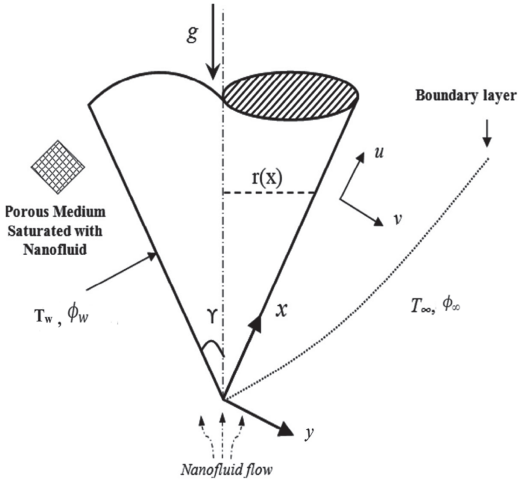

Fig. 1. Physical model and coordinate system.

Table I. Thermo-physical properties of water and nanoparticles.

Fluid	ρ (Kg/m^3)	C_p (J/kgK)	k (W/mK)	$\beta \times 10^5$ (K^{-1})
Pure water	997.1	4179	0.613	21
Copper (Cu)	8933	385	401	1.67
Silver (Ag)	10500	235	429	1.89
Alumina (Al_2O_3)	3970	765	40	0.85
Titanium Oxide (TiO_2)	4250	686.2	8.9538	0.9

approximation the governing equations take the following form:

$$\frac{\partial(ru)}{\partial x}+\frac{\partial(rv)}{\partial y}=0 \tag{1}$$

$$u\frac{\partial u}{\partial x}+v\frac{\partial u}{\partial y}=\frac{\mu_{nf}}{\rho_{nf}}\frac{\partial^2 u}{\partial y^2}-\frac{\mu_{nf}}{\rho_{nf}}\frac{1}{K}u+g[\beta(T-T_\infty) -\beta^*(\phi-\phi_\infty)]\cos\gamma-\frac{\sigma_{nf}B_0^2}{\rho_{nf}}u \tag{2}$$

$$u\frac{\partial T}{\partial x}+v\frac{\partial T}{\partial y}=\alpha_{nf}\frac{\partial^2 T}{\partial y^2}+\frac{1}{(\rho c_p)_{nf}}(q''')-\frac{1}{(\rho c_p)_{nf}}\frac{\partial q_r}{\partial y} \tag{3}$$

$$u\frac{\partial \phi}{\partial x}+v\frac{\partial \phi}{\partial y}=D_m\frac{\partial^2 \phi}{\partial y^2}-K_r(\phi-\phi_\infty) \tag{4}$$

The associated boundary conditions are

$$u=0,\quad v=0,\quad T=T_w,\quad \phi=\phi_w \quad \text{at } y=0 \tag{5}$$

$$u\to 0,\quad T\longrightarrow T_\infty,\quad \phi\longrightarrow\phi_\infty \quad \text{at } y\to\infty \tag{6}$$

The radiative heat flux q_r (using Rosseland approximation) is defined as

$$q_r=-\frac{4\sigma^*}{3K^*}\frac{\partial T^4}{\partial y} \tag{7}$$

We assume that the temperature variances inside the flow are such that the term T^4 can be represented as linear function of temperature, so, it has Taylor series expansion. After neglecting higher-order terms from the Taylor series expansion of T^4 about T_∞, we get

$$T^4\cong 4T_\infty^3T-3T_\infty^4 \tag{8}$$

Thus substituting Eq. (8) in Eq. (7), we get

$$q_r=-\frac{16T_\infty^3\sigma^*}{3K^*}\frac{\partial T}{\partial y} \tag{9}$$

The non-uniform heat source/sink, q''', is defined as

$$q'''=\frac{\kappa_f}{x\nu_f}[A1(T_w-T_\infty)f'+B1(T-T_\infty)]$$

where $A1$ and $B1$ are the coefficients of space and temperature-dependent heat source/sink, respectively. The case $A1>0$, $B1>0$ corresponds to internal heat source and the case $A1<0$, $B1<0$ corresponds to internal heat sink.

The dynamic viscosity μ_{nf}, density ρ_{nf}, thermal diffusivity α_{nf}, thermal conductivity k_{nf}, heat capacitance $(\rho c_p)_{nf}$, electrical conductivity σ_{nf} of the nanofluid and kinematic viscosity ν_f of the base fluid are defined as follows:

$$\alpha_{nf}=\frac{k_{nf}}{(\rho c_p)_{nf}},\quad \mu_{nf}=\frac{\mu_f}{(1-\varphi)^{2.5}},\quad \nu_f=\frac{\mu_f}{\rho_f},$$

$$\rho_{nf}=(1-\varphi)\rho_f+\varphi\rho_s,\quad (\rho c_p)_{nf}=(1-\varphi)(\rho c_p)_f+\varphi(\rho c_p)_s,$$

$$k_{nf}=k_f\left(\frac{k_s+2k_f-2\varphi(k_f-k_s)}{k_s+2k_f+2\varphi(k_f-k_s)}\right),$$

$$\frac{\sigma_{nf}}{\sigma_f}=1+\frac{3(\sigma_s/\sigma_f-1)\phi}{(\sigma_s/\sigma_f+2)-(\sigma_s/\sigma_f-1)\phi}$$

The following similarity transformations are introduced to simplify the mathematical analysis of the problem

$$\eta=\frac{y}{x}Ra_x^{1/4},\quad f(\eta)=\frac{\psi}{\alpha Ra_x^{1/4}},\quad \theta(\eta)=\frac{T-T_\infty}{T_w-T_\infty},\quad S(\eta)=\frac{\phi-\phi_\infty}{\phi_w-\phi_\infty} \tag{10}$$

Where Ra_x is the local Rayleigh number and is defined as

$$Ra_x=\frac{g\beta_{bf}\rho_{bf}(T-T_\infty)x^3\cos\gamma}{\mu_{bf}\alpha_{bf}}$$

and r can be approximated by the local radius of the cone, if the thermal boundary layer is thin, and is related to the x coordinate by $r=x\sin\gamma$.

Substituting Eq. (10) into Eqs. (1)–(4), we get the following system of non-linear ordinary differential equations

$$f'''+\frac{A_1}{Pr}\left[\frac{3}{4}ff''-\frac{1}{2}(f')^2\right]-k1f'-\frac{A_1}{A_2}Mf' +A_1[\theta-NrS]=0 \tag{11}$$

$$(1+R)\theta''+\frac{3}{4}A_3A_4f\theta'+A_4(Af'+B\theta)=0 \tag{12}$$

$$S''+\frac{3}{4}ScfS'-Cr.S=0 \tag{13}$$

The transformed boundary conditions are

$$\eta=0,\quad f=0,\quad f'=1,\quad \theta=1,\quad S=1$$
$$\eta\longrightarrow\infty,\quad f'=0,\quad \theta=0,\quad S=0 \tag{14}$$

where prime denotes differentiation with respect to η, and the significant thermophysical parameters dictating the flow dynamics are defined by

$$Nr=\frac{\beta^*(\phi_w-\phi_\infty)}{\beta(T_w-T_\infty)},\quad k1=\frac{x^2}{KRa_x^{1/2}},\quad Cr=\frac{K_rx^2}{D_mRa_x^{1/2}},$$

ARTICLE

$$Pr = \frac{\mu_f}{\alpha \rho_f}, \quad R = \frac{16T_\infty^3 \sigma^*}{3K^* k_{nf}}, \quad M = \frac{\sigma \beta_o^2 x^2}{\mu_f Ra_x^{1/2}},$$

$$Sc = \frac{\alpha}{D_m}, \quad A = \frac{A1x^2}{\gamma_f Ra_x^{1/2}}, \quad B = \frac{B1x^2}{\gamma_f Ra_x^{1/2}},$$

$$A_1 = (1-\varphi)^{2.5}\left[(1-\varphi) + \varphi\left(\frac{\rho_s}{\rho_f}\right)\right],$$

$$A_2 = (1-\varphi) + \varphi\left(\frac{\rho_s}{\rho_f}\right),$$

$$A_3 = (1-\varphi) + \varphi\left(\frac{(\rho C_p)_s}{(\rho C_p)_f}\right), \quad A_4 = \frac{k_f}{k_{nf}}$$

Quantities of practical interest in this problem are skin-friction coefficient, local Nusselt number Nu_x, and the local Sherwood number Sh_x, which are defined as

$$C_f = \frac{2\tau_w}{\rho U_\infty^2}, \quad Nu_x = \frac{xq_w}{k(T_w - T_\infty)}, \quad Sh_x = \frac{xJ_w}{D_B(\phi_w - \phi_\infty)} \tag{15}$$

The set of ordinary differential Eqs. (11)–(13) are highly non-linear, and therefore cannot be solved analytically. The finite-element method[39–42] has been implemented to solve these non-linear equations. The very important aspect in this numerical procedure is to select an approximate finite value of η_∞. So, in order to estimate the relevant value of η_∞, the solution process has been started with an initial value of $\eta_\infty = 10$, and then the Eqs. (11)–(13) are solved together with boundary conditions (14). We have updated the value of η_∞ and the solution process is continued until the results are not affected with further values of η_∞. The choice of $\eta_{\max} = 20$ and $\eta_{\max} = 8$ for velocity, temperature and concentration have confirmed that all the numerical solutions approach to the asymptotic values at the free stream conditions.

3. NUMERICAL METHOD OF SOLUTION

The finite-element method (FEM) is such a powerful method for solving ordinary differential equations and partial differential equations. The basic idea of this method is dividing the whole domain into smaller elements of finite dimensions called finite elements. The steps involved in the finite-element are as follows.

(i) Finite-element discretization
(ii) Generation of the element equations
(iii) Assembly of element equations
(iv) Imposition of boundary conditions
(v) Solution of assembled equations.

4. RESULTS AND DISCUSSION

The system of Eqs. (11)–(13) together with the boundary conditions (14) are solved for different values of the parameters that describe the flow characteristics and the results are illustrated graphically from Figures 2–13. The thermophysical properties of different nanofluids are shown in Table I. Comparison with previously published work is made and is shown in Table II.

The effect of magnetic field parameter (M) on the velocity and temperature profiles are depicted in Figures 2 to 3 for the both Al_2O_3-water and Cu-water based nanofluids. The velocity profile impedes throughout the boundary layer with the increase in the strength of magnetic parameter in both the Al_2O_3-water and Cu-water nanofluids

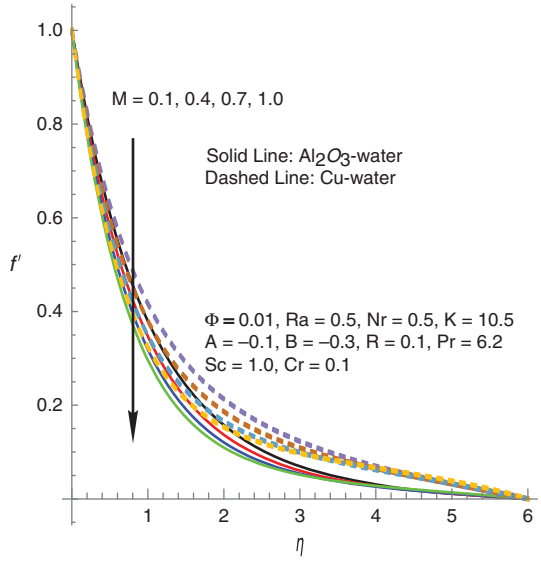

Fig. 2. Effect of (M) on velocity profiles.

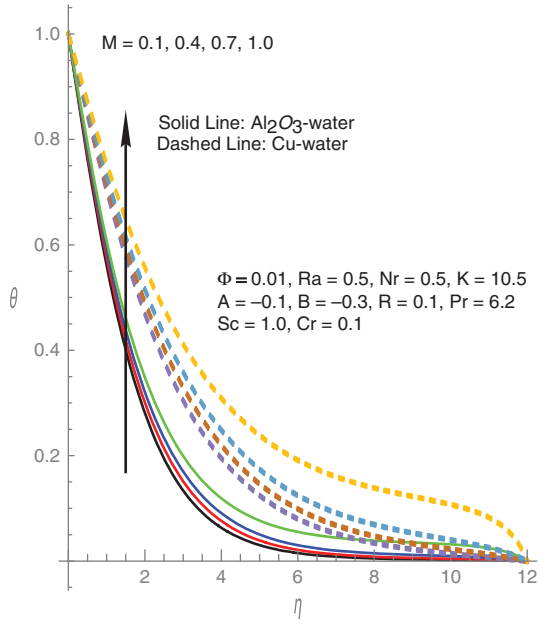

Fig. 3. Effect of (M) on temperature profiles.

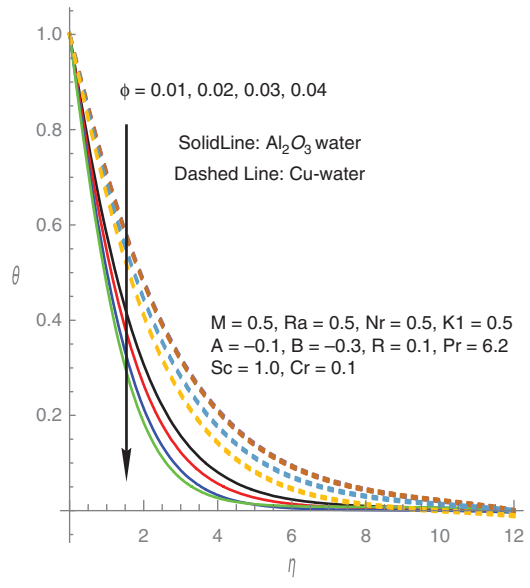

Fig. 4. Effect of (φ) on temperature profiles.

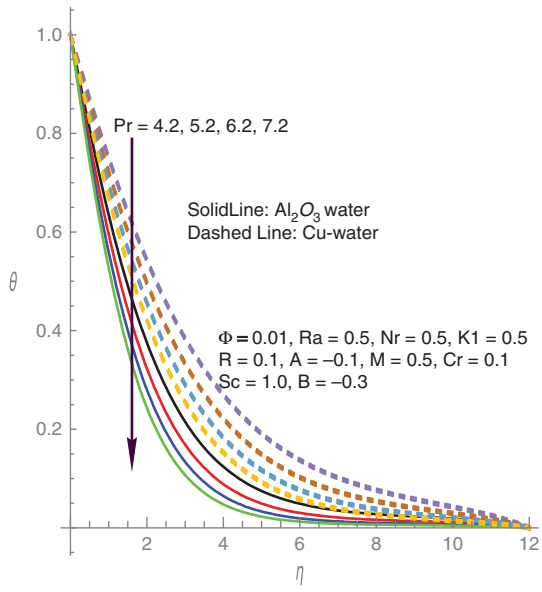

Fig. 6. Effect of (Pr) on temperature profiles.

(Fig. 2). We define the thermal energy as the additional force which drags the nanofluid from the influence of the magnetic field. This additional force increases the thickness of the thermal boundary layer, so that the temperature profile enriches with rise in M and this rise is more in the Cu-water nanofluid than the Al_2O_3-water nanofluids (Fig. 3).

Figures 4 to 5 shows the temperature (θ) and concentration (S) distributions for different values of the nanoparticle volume fraction parameter (φ) for the both Al_2O_3-water and Cu-water nanofluids. The temperature and concentration distributions are both decelerate with the increasing values of (φ) in the both Al_2O_3-water and Cu-water based nanofluid. This means that the thickness of the both thermal and solutal boundary layers is reduced in the fluid regime.

The temperature and concentration distributions for various values of the Prandtl number (Pr) are shown in Figures 6 to 7. We observe from Figure 6 that the temperature profiles decrease with higher Prandtl number values for both nanofluids. By definition, the Prandtl number is defined as the ratio of momentum diffusivity to the thermal diffusivity and therefore, increasing the values of Pr means a higher momentum diffusivity or a lesser thermal diffusivity which causes the reduction in the thermal boundary layer thickness and the deceleration in the

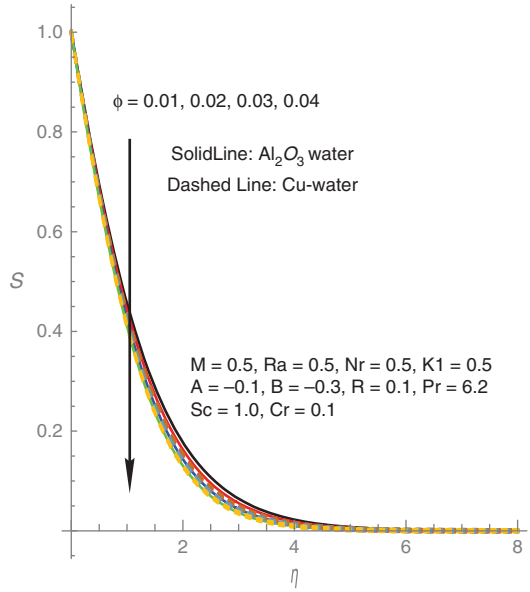

Fig. 5. Effect of (φ) on concentration profiles.

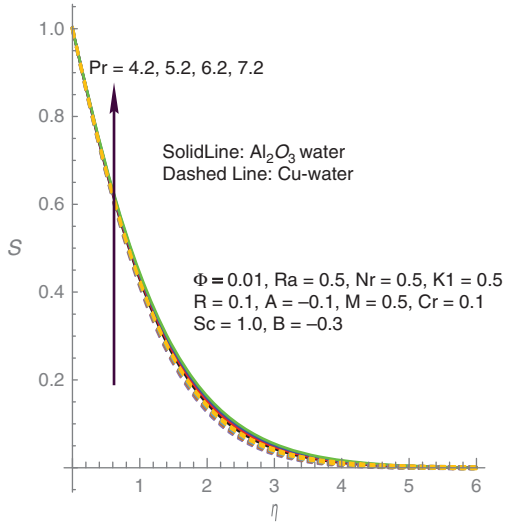

Fig. 7. Effect of (Pr) on concentration profiles.

ARTICLE

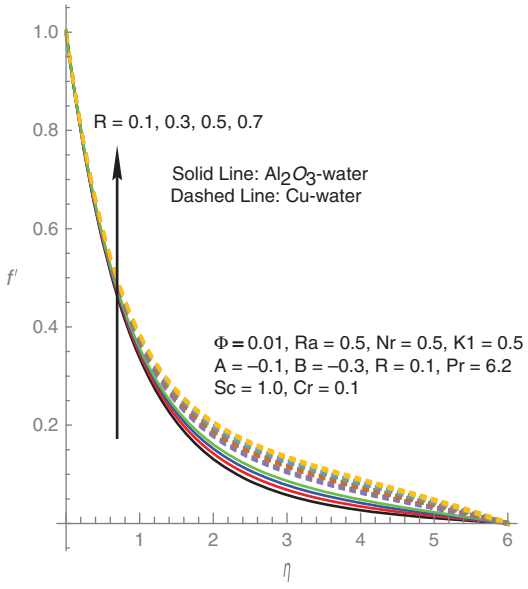

Fig. 8. Effect of R) on velocity profiles.

temperature profiles is higher in the Al_2O_3-water nanofluid than in the Cu-water nanofluid (Fig. 7).

The effect of the radiation parameter (R) on velocity and temperature profiles is shown in Figures 8 and 9 for the both nanofluids. It is seen that as the values of the thermal radiation parameter increases, the hydrodynamic and thermal boundary layer thickness is enhanced in the both nanofluids. This is due to the fact that the presence of the thermal radiation effect increases the temperature of the fluid in the entire flow region.

The velocity and temperature profiles of the Al_2O_3-water and Cu-water nanofluids for different values of the

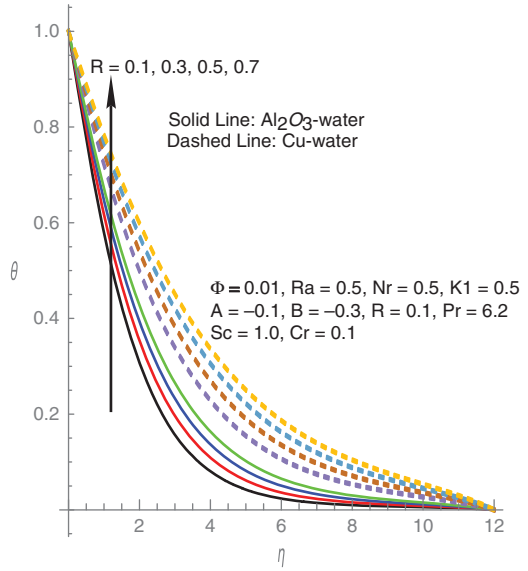

Fig. 9. Effect of (R) on temperature profiles.

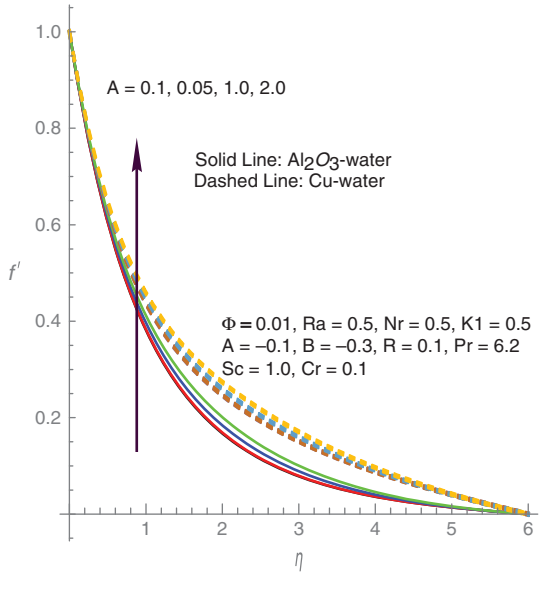

Fig. 10. Effect of (A) on velocity profiles.

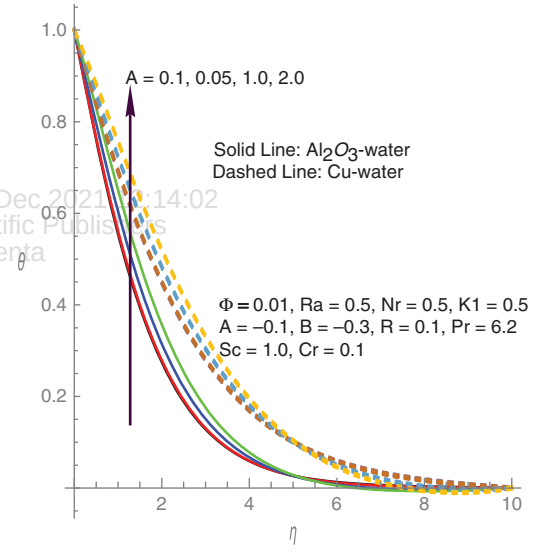

Fig. 11. Effect of (A) on temperature profiles.

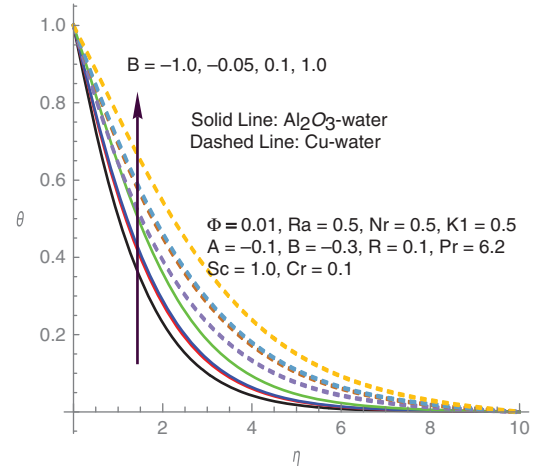

Fig. 12. Effect of (B) on temperature profiles.

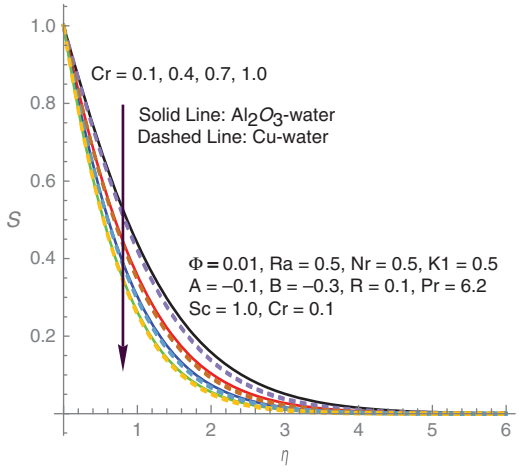

Fig. 13. Effect of (Cr) on concentration profiles.

Table II. Comparison of $-f''(0)$, $-\theta'(0)$ with previously published data for $Pr = 6.2$, $k_1 = 0$, $R = 0$, $Nr = 0$, $Sc = 0$, $A = 0$, $B = 0$, $Cr = 0$.

$-f''(0)$				$-\theta'(0)$	
Parameter		Hamad[43]	Present study	Hamad[43]	Present study
M	φ	Al_2O_3	Al_2O_3	Al_2O_3	Al_2O_3
0	0.05	1.00538	1.00532	1.62246	1.62245
	0.10	0.99877	0.99875	1.49170	1.49175
	0.15	0.98185	0.98184	1.37543	1.37542
	0.20	0.95592	0.95590	1.27118	1.27116

space-dependent coefficient parameter (A) are depicted in Figures 10 and 11. The both velocity and temperature distributions enhance in the boundary layer regime with increasing values of (A) for both heat generation and heat absorption cases. The impact of temperature-dependent coefficient (B) for heat a source/sink on temperature distributions is depicted in Figure 12. It is observed that temperature in the thermal boundary layer increases with increase in (B) (positive values), whereas the thermal boundary layer thickness decelerates with the decrease in the heat absorption parameter (B) (negative values).

Figure 13 illustrates the effect of the chemical reaction parameter Cr on the concentration distributions for both Al_2O_3-water and Cu-water nanofluids. We see from this figure that the concentration profiles impede with rising values of the chemical reaction parameter in the flow region.

The values of skin-friction coefficient $(-f''(0))$, local Nusselt number $(-\theta'(0))$, and local Sherwood number $(-\phi'(0))$ for the both Al_2O_3-water and Cu-water nanofluids are calculated and presented in Table III. It is evident that the local skin-friction coefficient enhances whereas dimensionless heat and mass transfer rates decrease in the both Al_2O_3-water and Cu-water based nanofluids with increasing values of the magnetic field parameter (M). It is found that the rate of heat transfer and mass transfer decreases in the both Cu-water and Ag-water based nanofluids, but reserve trend is observed in skin-friction coefficient with the increasing values of nanoparticle volume fraction parameter ϕ. It is also noted from this table that skin-friction coefficient and heat transfer rates retards, whereas mass transfer rates raises in both the Al_2O_3-water and Cu-water based nanofluids with increasing values of thermal radiation parameter (R). It is reported that rate of velocity depreciates in the Cu-water based nanofluids whereas it increases in the Ag-water based nanofluids with higher values of (Cr). Dimensionless heat transfer rates rise in the Cu-water based nanofluids whereas it impedes in the Ag-water nanofluid with increasing values of chemical reaction parameter (Cr). Sherwood number rises in the both nanofluids with (Cr).

Table III. Effect of various parameters on Skin-friction coefficient $(-f''(0))$ local Nusselt number $(-\theta'(0))$) and local Sherwood number $(-\varphi'(0))$.

Parameter				$-f''(0)$		$-\theta'(0)$		$-\varphi'(0)$	
M	φ	R	Cr	Al_2O_3	Cu	Al_2O_3	Cu	Al_2O_3	Cu
0.1	0.01	0.1	0.1	1.01431	0.97482	0.49084	0.31626	0.67366	0.68898
0.5	0.01	0.1	0.1	1.11614	1.07839	0.47354	0.30166	0.65936	0.67407
0.7	0.01	0.1	0.1	1.21037	1.17657	0.45705	0.28654	0.64667	0.66065
1.0	0.01	0.1	0.1	1.29734	1.26555	0.43626	0.26152	0.63594	0.64987
0.5	0.01	0.1	0.1	1.14833	0.94507	0.46802	0.30868	0.65496	0.68645
0.5	0.02	0.1	0.1	0.99597	0.97550	0.51035	0.31226	0.67280	0.68168
0.5	0.03	0.1	0.1	0.84003	0.83044	0.56129	0.33590	0.69595	0.69961
0.5	0.04	0.1	0.1	0.74516	0.74349	0.59870	0.36021	0.71197	0.71266
0.5	0.01	0.1	0.1	1.14833	1.11692	0.46802	0.29651	0.65496	0.66895
0.5	0.01	0.3	0.1	1.13967	1.10531	0.42031	0.26681	0.65857	0.67226
0.5	0.01	0.5	0.1	1.13254	1.10000	0.38330	0.24387	0.66158	0.67451
0.5	0.01	0.7	0.1	1.12655	1.05700	0.35362	0.22567	0.66412	0.67633
0.5	0.01	0.1	0.1	1.04128	0.98206	0.49125	0.32426	0.67549	0.69705
0.5	0.01	0.1	0.4	1.02721	0.96602	0.49597	0.32692	0.87924	0.89158
0.5	0.01	0.1	0.7	1.01772	0.95718	0.49872	0.32853	1.04113	1.04960
0.5	0.01	0.1	1.0	1.01055	0.95038	0.50059	0.32964	1.17977	1.18618

ARTICLE

ARTICLE

5. CONCLUSIONS

In the present paper, we have analyzed the heat and mass transfer characteristics of Cu-water and Al_2O_3-water nanofluids through porous medium over a vertical cone by taking thermal radiation, magnetic field, heat source/sink parameters and chemical reaction effect into the consideration. The conservation equations of mass, momentum, energy and nanoparticle volume concentration together with the boundary conditions are transformed into a set of highly non-linear ordinary differential equations with the help of similarity transformations. These transformed equations are solved numerically using an extensively validated, highly efficient, most suitable variational Finite Element Method (FEM). The important conclusions given by the numerical solutions of the problem are as follows.

(i) Velocity profiles depreciate, whereas temperature and concentration profiles elevates with (M) in the both nanofluids.

(ii) When the values of (φ) increases then velocity distributions rises whereas temperature, concentration profiles depreciates in the boundary layer regime.

(iii) Temperature profiles improves with space-dependent (A) and temperature-dependent (B) for heat source/sink parameters.

(iv) As the values of (R) increases both velocity and temperature profiles elevates in both the nanofluids.

(v) The concentration profiles are highly influenced by the chemical reaction parameter in the flow region.

Nomenclature

Ra_x Rayleigh number
k_s Thermal conductivity of nanoparticle
ϕ Nanoparticle volume fraction
ϕ_∞ Ambient nanoparticle volume fraction
T_w Temperature at the cone surface
T Fluid temperature
q_w Wall heat flux
$f(\eta)$ Dimensionless stream function
P Pressure
K^* Mean absorption coefficient
M Magnetic parameter
Cr Chemical reaction parameter
Nr Buoyancy ratio parameter
(u, v) Velocity components in x- and y-axis
C_f Skin-friction coefficient
a Constant
B Temperature-dependent heat source/sink
q''' Non-uniform heat source/sink
K Permeability parameter
C_f Skin-friction coefficient
Nu_x Nusselt number
ϕ_w Nanoparticle volume fraction on the cone
(x, y) Cartesian coordinates
T_∞ Ambient temperature attained
K_r Rate of chemical reaction
J_w Wall mass flux
g Gravitational acceleration
B_0 Magnetic field strength
q_r Radiative heat flux
σ^* Stephan-Boltzmann constant
Sh_x Sherwood number
Pr Prandtl number
R Radiation parameter
τ_w Shear stress
A Space-dependent heat source/sink
Sc Schmidt number
D_m Mean fluid concentration.

Greek Symbols

α Thermal diffusivity of base fluid
ρ_f Fluid density
ψ Stream function
τ Parameter defined by $\varepsilon((\rho c)_p/(\rho c)_f)$
ϕ (η) Dimensionless nanoparticle volume fraction
θ (η) Dimensionless temperature
β Thermal expansion coefficient
$(\rho c_p)_p$ Heat capacitance of the nanofluid
ρ_{nf} Density of the nanofluid
σ Electrical conductivity
ν_f Kinematic viscosity of the base fluid
ρ_p Nanoparticle mass density
$(\rho c_p)_f$ Heat capacitance of the base fluid
$(\rho)_f$ Density of the base fluid
η Similarity variable
$(\rho)_p$ Density of the nanofluid
σ Electrical conductivity
$(\mu)_{nf}$ Viscosity of the nanofluid
$(\rho c_p)_{nf}$ Heat capacitance of the nanofluid
k_{nf} Thermal conductivity of nanofluid.

Subscripts

w Condition at cone surface
η Similarity variable
∞ Condition far away from cone surface
f Base fluid.

References and Notes

1. S. K. Das, S. Choi, W. Yu, and T. Pradeep, Science and Technology, Wiley Interscience, New York **(2008)**.
2. R. Saidur, K. Y. Leong, and H. A. Mohammad, *Renew. Sustain. Energy Rev.* 15, 1646 **(2011)**.
3. S. U. S. Choi, Enhancing thermal conductivity of fluids with nanoparticles, developments and applications of non-Newtonian flows, *FED—Vol. 231/MD*, edited by D. A. Siginer and H. P. Wang, The American Society of Mechanical Engineers, New York **(1995)**, Vol. 66, pp. 99–105.
4. J. A. Eastman, S. U. S. Choi, S. Li, L. J. Thompson, and S. Lee, Enhanced thermal conductivity through the development of nanofluids, edited by S. Komarneni, J. C. Parker, and H. J. Wollenberger, Nanophase and Nanocomposite Materials II, MRS, Pittsburg, PA **(1997)**, pp. 3–11.

5. J. A. Eastman, S. U. S. Choi, S. Li, W. Yu, and L. J. Thompson, *Appl. Phys. Lett.* 78, 718 **(2001)**.
6. S. U. S. Choi, Z. G. Zhang, W. Yu, F. E. Lockwood, and E. A. Grulke, *Appl. Phys. Lett.* 79, 2252 **(2001)**.
7. H. Xie, J. Wang, T. Xi, Y. Liu, F. Ai, and Q. Wu, *J. Appl. Phys.* 91, 4568 **(2002)**.
8. J. Buongiorno, *J. Heat Transfer* 128, 240 **(2006)**.
9. N. Putra, W. Roetzel, and S. K. Das, *Heat Mass Transf.* 39, 775 **(2003)**.
10. D. Wen and Y. Ding, *Int. J. Heat Fluid Flow* 26, 855 **(2005)**.
11. C. H. Li and G. P. Peterson, *Advances in Mechanical Engineering* Article ID 742739 **(2010)**.
12. N. Rui, Z. Sheng-Qi, and X. Ke-Qing, *Physics of Fluids* 23, Article ID 022005 **(2011)**.
13. A. G. A. Nnanna, *J. Heat Transf.* 129, 697 **(2007)**.
14. C. J. Ho, W. K. Liu, Y. S. Chang, and C. C. Lin, *Int. J. Therm. Sci.* 49, 1345 **(2010)**.
15. M. Ghalambaz, A. Behseresht, A. Behseresht, and A. J. Chamkha, *Advanced Powder Technology* 26, 224 **(2015)**.
16. A. Lervik, F. Bresme, and S. Kjelstrup, *Soft Matter.* 12, 2407 **(2009)**.
17. E. Abu-Nada, Z. Masoud, and A. Hijazi, *Int. Commun. Heat Mass Transfer* 35, 657 **(2008)**.
18. C. Eliodoro, F. Matteo, A. Pietro, and D. Paolo, *Nature Communications* 5, Article ID 3565. **(2014)**.
19. K. Khanafer, K. Vafai, and M. Lightstone, *Int. J. Heat Mass Transfer* 46, 3639 **(2003)**.
20. H. F. Oztop and E. Abu-Nada, *Int. J. Heat Fluid Flow* 29, 1326 **(2008)**.
21. S. M. Aminossadati and B. Ghasemi, *European J. Mechanics-B/Fluids* 28, 630 **(2009)**.
22. B. Ghasemi and S. M. Aminossadati, *Int. J. Therm. Sci.* 49, 931 **(2010)**.
23. O. Fakhreddine Segni and B. Rachid, *Nanoscale Research Letters* 6, Article ID 222 **(2011)**.
24. P. Ternik and R. Rudolf, *Int. J. Simulation Modelling* 11, 29 **(2012)**.
25. A. J. Chamkha, S. Abbasbandy, A. M. Rashad, and K. Vajravelu, *Transport in Porous Media* 91, 261 **(2012)**.
26. A. J. Chamkha, S. Abbasbandy, A. M. Rashad, and K. Vajravelu, *Meccanica* 48, 275 **(2012)**.
27. A. J. Chamkha and A. M. Rashad, *The Canadian Journal of Chemical Engineering* 92, 758 **(2014)**.
28. A. Noghrehabadi, R. Pourrajab, and M. Ghalambaz, *International Journal of Thermal Sciences* 54, 253 **(2013)**.
29. A. Noghrehabadi, M. R. Saffarian, R. Pourrajab, and M. Ghalambaz, *Journal of Mechanical Science and Technology* 27, 927 **(2013)**.
30. A. Noghrehabadi, A. Behseresht, and M. Ghalambaz, *Applied Mathematics and Mechanics* 34, 669 **(2013)**.
31. A. Behseresht, A. Noghrehabadi, and M. Ghalambaz, *Chemical Engineering Research and Design* 92, 447 **(2013)**.
32. AM. Rashad, S. Abbasbandy, and A. J. Chamkha, *ASME Journal of Heat Transfer* 136, 22503-1-9 **(2014)**.
33. M. Ghalambaz, A. Noghrehabadi, and A. Ghanbarzadeh, *Brazilian Journal of Chemical Engineering* 31, 413 **(2014)**.
34. P. Sudarsana Reddy and K. V. Suryanarayana Rao, *Procedia Engineering* 127, 476 **(2015)**.
35. Noreen Sher Akbar, M. Raja, and R. Ellahi, *Journal of Magnetism and Magnetic Materials* 381, 405 **(2015)**.
36. M. Sheikholeslami, M. G. Bandpy, R. Ellahi, and A. Zeeshan, *Journal of Magnetism and Magnetic Materials* 369, 69 **(2014)**.
37. M. Sheikholeslami, D. D. Ganji, M. Younus Javed, and R. Ellahi, *Journal of Magnetism and Magnetic Materials* 374, 36 **(2015)**.
38. A. V. Kuznetsov and D. A. Nield, *International Journal of Thermal Sciences* 49, 243 **(2010)**.
39. R. Bhargava, R. Sharma, and O. A. Bég, *Int. J. Appl. Math. Mech* 5, 15 **(2009)**.
40. O. Anwar Bég, H. S. Takhar, R. Bhargava, S. Rawat, and V. R. Prasad, *Phys. Scr.* 77, 1 **(2008)**.
41. P. S. Reddy and A. J. Chamkha, *Advanced Powder Technology* **(2016)**, 10.1016/j.apt.2016.04.005.
42. P. Rana and R. Bhargava, *Comm. Nonlinear Sci. Numer. Simulat.* 17, 212 **(2012)**.
43. M. A. A. Hamad, *International Communications in Heat and Mass Transfer* 38, 487 **(2011)**.